

Cluster-guided Asymmetric Contrastive Learning for Unsupervised Person Re-Identification

Mingkun Li,
School of Information and
Communication Engineering,
Beijing University of
Posts and Telecommunications
mingkun.li@bupt.edu.cn

Chun-Guang Li
School of Information and
Communication Engineering,
Beijing University of
Posts and Telecommunications
lichunguang@bupt.edu.cn

Jun Guo
School of Information and
Communication Engineering,
Beijing University of
Posts and Telecommunications
guojun@bupt.edu.cn

Abstract

Unsupervised person re-identification (Re-ID) aims to match pedestrian images from different camera views in unsupervised setting. Existing methods for unsupervised person Re-ID are usually built upon the pseudo labels from clustering. However, the quality of clustering depends heavily on the quality of the learned features, which are overwhelmingly dominated by the colors in images especially in the unsupervised setting. In this paper, we propose a Cluster-guided Asymmetric Contrastive Learning (CACL) approach for unsupervised person Re-ID, in which cluster structure is leveraged to guide the feature learning in a properly designed asymmetric contrastive learning framework. To be specific, we propose a novel cluster-level contrastive loss to help the siamese network effectively mine the invariance in feature learning with respect to the cluster structure within and between different data augmentation views, respectively. Extensive experiments conducted on three benchmark datasets demonstrate superior performance of our proposal.

1. Introduction

Unsupervised person Re-identification (Re-ID) aims to match pedestrian images from different camera views in unsupervised setting without demanding of massive labeling data, and has attracted increasing attention in com-

puter vision and pattern recognition community in recent years [40]. The great challenge we have to face in unsupervised person Re-ID is to tackle with the heavy variations from different viewpoints, varying illuminations, changing weather conditions, clutter background and etc., without supervision.

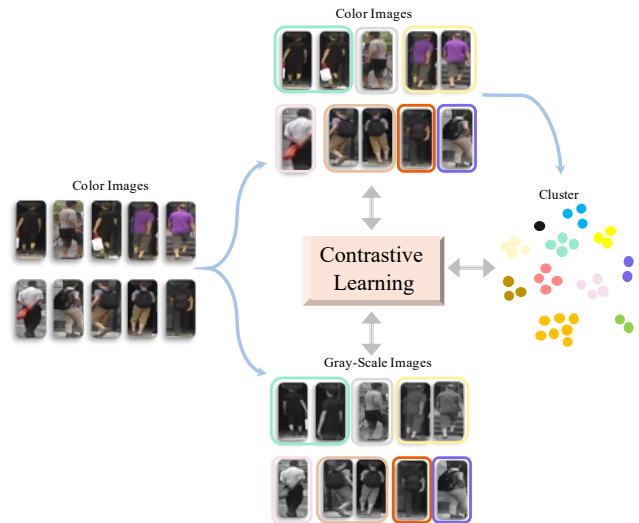


Figure 1. Illustration for Our Proposal. We attempt to leverage the cluster structure into contrastive learning (via a siamese network) to find more effective features with invariance between the color images and gray-scale images.

Existing methods for unsupervised person Re-ID are usually built on exploiting weak supervision information (e.g., pseudo labels) from clustering. For example, MMT [13] uses DBSCAN [8] algorithm to generate pseudo labels and exploit the pseudo labels to train two networks. HCT [36] uses a hierarchical clustering algorithm to gradually assign pseudo labels to the train samples during training period. SSG [11] uses k -means on training sample with multi-views. However, the performance of these methods relies on the quality of the pseudo labels, which directly depends on the feature representation of the images.

Recently, contrastive learning is exploited to perform feature learning in unsupervised setting, e.g., [33, 3, 4, 5, 15]. The primary idea in these methods is to learn some invariance in feature representation with self-supervised mechanism based on data augmentation. In SimCLR [4], each sample and its multiple augmentations are treated as positive pairs and the rest of the samples in the same batch are treated as negative pairs, and uses a contrastive loss to distinguish the positive and negative samples to prevent the model from falling into a trivial solution. While promising performance is achieved, SimCLR needs a large batch size, e.g., 256 ~ 4096, to contain enough negative samples for effectively training the networks. In BYOL [15] and SimSiam [5], a predictor layer is used to prevent the collapse without using negative samples. In InterCLR [33] and SwAV [3], clustering is exploited to prevent collapse. In particular, in SwAV [3], a scalable online clustering loss is proposed to train the siamese network with multi-crop data augmentation; whereas in InterCLR [33], a Margin-NCE loss is proposed to enhance the discriminant power. However, the initial training stage in [33, 3] are not stable and robust, leading to a dramatically degenerated performance.

In this paper, we attempt to leverage the idea in contrastive learning to develop effective approach for unsupervised person Re-ID. However, in person Re-ID, the difference between images of different pedestrians is much smaller than that between natural images (e.g., different species or different categories). Simply selecting negative samples as in [4] is ineffective due to destroying the hidden structure in samples of similar appearance. The performance of person Re-ID depends heavily on the effectiveness of the learned features, however, the learned features are overwhelmingly dominated by the colors in pedestrian images especially in the unsupervised setting. While color is an important feature to match pedestrian images in person Re-ID, unfortunately, it is also an obstacle to learn more effective texture feature other than colors. When different people are wearing clothes in the same or similar color, the texture features, rather than the colors, are discriminative to distinct different individuals. Thus, exploring more stable and discriminative feature that is invariant or resisted to

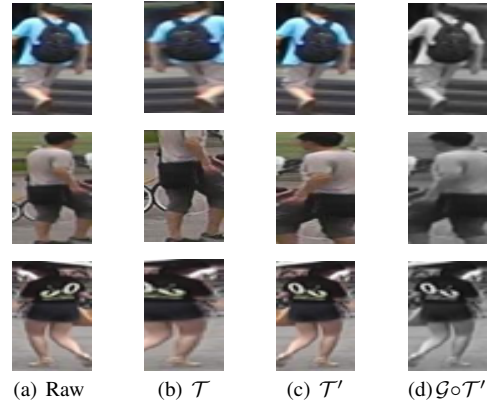


Figure 2. Illustration for the raw images and the augmented images. The first column shows the raw images. The middle two columns show the images generated with transform $\mathcal{T}(\cdot)$ and $\mathcal{T}'(\cdot)$. The last column shows the corresponding gray-scale images which process are generated with both transform $\mathcal{T}'(\cdot)$ and color-to-grayscale transform $\mathcal{G}(\cdot)$, i.e., $\mathcal{G} \circ \mathcal{T}'(\cdot)$.

dominating colors is helpful to develop robust feature for person Re-ID. However, to the best of our knowledge, there is no prior work in unsupervised person Re-ID in this line to date.

We attempt to leverage the clustering structure in samples into a properly designed asymmetric contrastive learning framework to learn effective features for person Re-ID in unsupervised setting, as shown in Fig. 1. The clustering structure provides weak supervision to guide contrastive learning without negative sample pairs, and at the same time, samples in different views via special transforms of data augmentation (color images vs. gray-scale images as shown in Fig. 2) provide strong supervision to impose invariance in feature learning.

Specifically, in this paper, we propose an approach for unsupervised person Re-ID, termed Cluster-guided Asymmetric Contrastive Learning (CACL). As shown in Fig. 3, our proposed CACL is a siamese network, where input images transformed via different data augmentation are provided into both network branches. We note that CACL is asymmetry in two aspects: a) asymmetry in network structure, i.e., a predictor layer is added after the first branch; and b) asymmetry in data augmentation, i.e., the samples provided to the second branch are further processed into gray-scale. To prevent collapsing into a trivial solution, we propose a cluster-level contrastive loss, which exploits the pseudo labels obtained from the clustering result with the features of the first branch to perform contrastive learning with respect to cluster structure. By combining both cluster structure and contrastive learning, the proposed CACL is able to effectively recognize the samples with high different augmented views with the self-supervision and mine

the invariance between the instance-level and cluster-level at the same time.

Paper Contributions. The contribution of the paper is highlighted as follows.

1. We propose an unsupervised approach for person Re-ID that leverages cluster structure into an asymmetric contrastive learning framework to perform effective feature learning.
2. We propose a novel contrastive loss function that exploits both the cluster structure and the invariance in augmented data to conduct effective contrastive learning for person Re-ID.
3. We conduct extensive experiments on three benchmark data sets and achieved new state-of-art performance.

2. Related Work

2.1. Unsupervised Person Re-identification

Person Re-ID aims to find specific pedestrians from videos or pictures according to targets. For the increasing demand in real life and avoiding the high consumption of labeling datasets, unsupervised person re-identification has become popular in recent years [40]. The existing unsupervised person Re-ID methods can be divided into two categories: a) unsupervised domain adaptation methods, which need labeled source dataset and unlabeled target dataset [25, 1, 26, 30]; and b) pure unsupervised methods, which need with only unlabeled dataset [14, 23, 9, 24].

The unsupervised domain adaptation methods train the network with the help of labeled datasets, and transfer the network to unlabeled datasets by reducing the gap between two datasets, e.g., [28] proposed to align the second-order statistics of the distributions in the two domains through linear transformations to reduce the domain shift, [14] proposed a combined loss function to co-train with samples from the source and target domains and the merging memory bank, [12] proposed to maximize the inter-domain classification loss and minimize the intra-domain classification loss to learn domain robust features. However, unsupervised domain adaptation methods are limited by the distribution of source dataset and target dataset.

Most purely unsupervised person Re-ID methods rely on the pseudo label to train the network, e.g., HCT [36] uses a hierarchical clustering to generate pseudo labels and train the convolution neural network for feature learning, [29] assigns multiple labels to samples and proposes a new loss function for multi-label training. Note that the quality of the pseudo label relies on the feature representation of the input images, however, in the early stage, the feature representation is not good to generate high quality pseudo labels and the low quality pseudo labels will also contaminate the network training.

2.2. Contrastive Learning

In recent years, with the development and application of the siamese network, contrastive learning began to emerge in the field of unsupervised learning. Contrastive learning aims at learning good image representation. It learns invariance in features by manipulating a set of positive samples and negative samples with data augmentation. The existing methods of contrastive learning can be further categorized to: a) instance-level methods [4, 5, 2, 7, 15] and b) cluster-level methods [3, 33]. Instance-level methods regard each image as an individual class and consider two augmented views of the same image as positive pairs and treat others in the same batch (or memory bank) as negative pairs. For example, SimCLR [4] regards samples in the current batch as the negative samples. MoCo [16] uses a dictionary to implement contrast learning, which converts one branch of contrast learning into a momentum encoder. SimSiam [5] proposed a stop-gradient method that can train the siamese network without negative samples. Cluster-level methods regard samples in same clusters as positive cluster and other samples as negative clusters. InterCLR [33] combines InfoNCE loss with MarginNCE loss to both attract positive samples and repelled negative samples. SwAV [3] uses multi-crop data augmentation to enhance the robustness of the network, and proposed a scalable online clustering loss to enhance the ability of the network to explore the inter-invariance of clusters. However, in unsupervised setting, the instance-level contrastive learning methods simply make each sample independent and repel to each other, which will undoubtedly ignore the cluster structure information in samples; whereas the cluster-level contrastive learning methods rely on the clustering results in which the feature learning lacks of effective guide information in the early training stage.

Therefore, we attempt to combine the two lines of contrastive learning methods into a unified framework to form an effective mutual learning: the instance-level contrastive learning helps the network training to perform feature learning especially in the early training stage; whereas the cluster-level contrastive learning helps the network training especially when the quality of clustering is improved. In this way, the self-supervision information between different augmented views and the weak supervision information obtained from clustering is fully exploited without using negative samples.

3. Our Proposal: Cluster-guided Asymmetric Contrastive Learning (CACL)

This section will present our proposal—Cluster-guided Asymmetric Contrastive Learning (CACL) for unsupervised person Re-ID.

For clarity, we show the architecture of our proposed

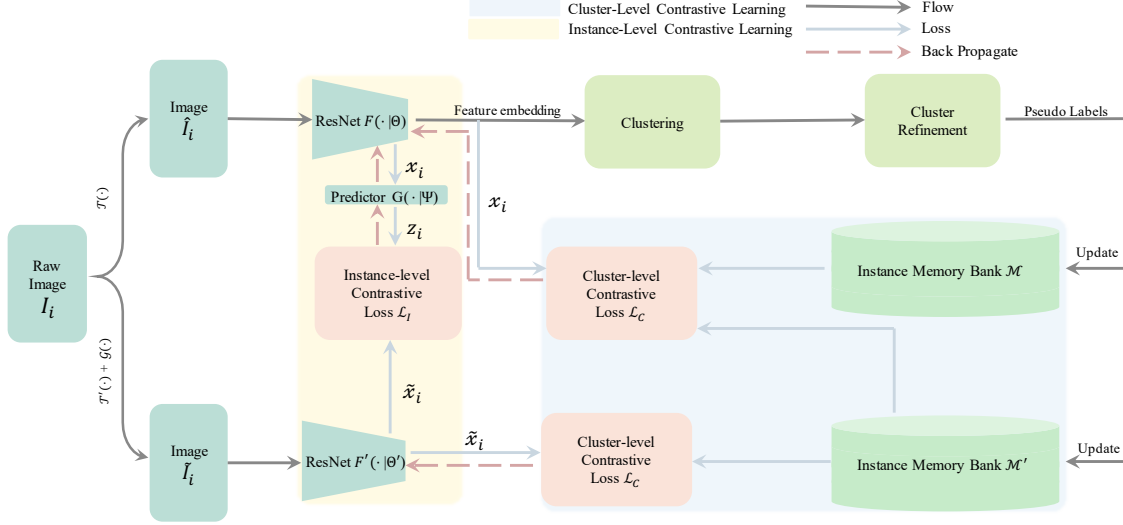


Figure 3. Illustration for Our Proposal: Cluster-guided Asymmetric Contrastive Learning Framework

CACL in Fig. 3. Overall, our CACL is a siamese network, which consists of two branches of backbone networks $F(\cdot|\Theta)$ and $F'(\cdot|\Theta')$ without sharing parameters, where Θ and Θ' are the parameters in the two networks, respectively, and a predictor layer $G(\cdot|\Psi)$ is added after the first branch where Ψ denotes the parameters. The backbone networks are $F(\cdot|\Theta)$ and $F'(\cdot|\Theta')$ implemented via ResNet-50 [17] for feature learning.

Given an unlabeled dataset $\mathcal{I} = \{I_i\}_{i=1}^N$ consisting of N image samples. For an input image $I_i \in \mathcal{I}$, we generate two samples \hat{I}_i and \tilde{I}_i via different data augmentation strategies¹, in which $\hat{I}_i = \mathcal{T}(I_i)$ and $\tilde{I}_i = \mathcal{G}(\mathcal{T}(I_i))$ where $\mathcal{T}(\cdot)$ and $\mathcal{T}'(\cdot)$ denote the different implementations of data augmentation and \mathcal{G} denotes the operation to transform color image into gray-scale image. For the first branch, we use \hat{I}_i as the input; whereas for the second branch, we use \tilde{I}_i as the input. For simplicity, we denote the output features of the first network branch and the second network branch as x_i and \tilde{x}_i , respectively, where $x_i, \tilde{x}_i \in \mathbb{R}^D$, and denote the output of the predictor layer in the first branch as z_i , where $z_i \in \mathbb{R}^D$.

To guide the contrastive learning, we perform clustering with the output features $\mathcal{X} := \{x_1, \dots, x_N\}$ of the first network branch to generate pseudo labels $\mathcal{Y} := \{y_1, \dots, y_N\}$ and exploit the pseudo labels to leverage the cluster structure into the contrastive learning. Specifically, in the training stage, the two network branches $F(\cdot|\Theta)$ and $F'(\cdot|\Theta')$ are trained with the manipulated samples with different data augmentation methods without sharing parameters, and the pseudo labels in \mathcal{Y} are used to guide the training of both network branches and also used to update the

¹Following SpCL [14], we use random horizontal flip, random erasing and random crop to define data augmentation $\mathcal{T}(\cdot)$ and $\mathcal{T}'(\cdot)$.

instance memory banks \mathcal{M} and $\tilde{\mathcal{M}}$, which are initialized with the initial features of the two network branches, respectively.

3.1. Clustering and Cluster Refinement

At beginning, we pre-train the two network branches $F(\cdot|\Theta)$ and $F'(\cdot|\Theta')$ on ImageNet [20], and employ clustering algorithm [8] with the features from the first network branch $F(\cdot|\Theta)$ to yield m clusters, which are denoted as $\mathcal{C} := \{\mathcal{C}^{(1)}, \mathcal{C}^{(2)}, \dots, \mathcal{C}^{(m)}\}$. The clustering result is used to generate pseudo labels to train the cluster-guided contrastive learning module.

Since that the quality of the pseudo labels is critical in unsupervised setting, we use a post-process step to refine the clustering result. Basically, we select larger clusters that contain samples with higher intra-similarity and remove lower intra-similarity samples as noisy samples.

At first, we over-segment $\{\mathcal{C}^{(1)}, \mathcal{C}^{(2)}\}$ into a set of clusters of smaller sizes. For example, cluster $\mathcal{C}^{(i)}$ is over-segmented to n_i sub-clusters (including singletons), denoted as $\{\mathcal{C}_1^{(i)}, \mathcal{C}_2^{(i)}, \dots, \mathcal{C}_{n_i}^{(i)}\}$. To judge whether $\mathcal{C}_j^{(i)}$ should be removed from cluster $\mathcal{C}^{(i)}$, we define a score for each $\mathcal{C}_j^{(i)}$ as follows:

$$\rho(\mathcal{C}_j^{(i)}|\mathcal{C}^{(i)}) = \frac{D_{sub}(\mathcal{C}_j^{(i)})}{D_{large}(\mathcal{C}^{(i)})} \quad (1)$$

where $D_{sub}(\cdot)$ is the average inter-distance from all samples in the sub-cluster $\mathcal{C}_j^{(i)}$ to other samples in cluster $\mathcal{C}^{(i)}$, and $D_{large}(\mathcal{C}^{(i)})$ is the average intra-distance in cluster $\mathcal{C}^{(i)}$.

Then, if $\rho(\mathcal{C}_j^{(i)}|\mathcal{C}^{(i)}) < 1$, we do not remove sub-cluster $\mathcal{C}_j^{(i)}$ from the large cluster $\mathcal{C}^{(i)}$; else, if $\rho(\mathcal{C}_j^{(i)}|\mathcal{C}^{(i)}) \geq 1$,

we remove sub-cluster $\mathcal{C}_j^{(i)}$ from cluster $\mathcal{C}^{(i)}$. Those sub-clusters removed from larger clusters forms tiny clusters or singletons.

After such a post-processing step, the clusters with larger sizes are improved and at the meantime, more singletons or tiny clusters are produced. We denote the refined clusters as $\mathcal{C}' = \{\mathcal{C}^{(1)}, \mathcal{C}^{(2)}, \dots, \mathcal{C}^{(m')}\}$. Compared to tiny clusters and singletons, the clusters with larger sizes are more informative to provide cluster structure to guide contrastive learning.

3.2. Cluster-guided Contrastive Learning

To exploit the invariance between the two augmented views and leverage the cluster structure, we employ two types of contrastive losses: a) instance-level contrastive loss, denoted as \mathcal{L}_I , and b) cluster-level contrastive loss, denoted as \mathcal{L}_C .

Instance-Level Contrastive Loss. To match the feature outputs z_i and \tilde{x}_i of the two network branches at instance-level, similar to [4, 15], we define an instance-level contrastive loss \mathcal{L}_I as the negative cosine similarity of the prediction outputs z_i in the first branch and the feature output of the second branch \tilde{x}_i as follows:

$$\mathcal{L}_I := -\frac{z_i^\top \tilde{x}_i}{\|z_i\|_2 \|\tilde{x}_i\|_2}, \quad (2)$$

where $\|\cdot\|_2$ is the ℓ_2 -norm.

Cluster-Level Contrastive Loss. To leverage the cluster structure to further explore the hidden information from different views, we propose a cluster-level contrastive loss \mathcal{L}_C , which is further divided to inter-views cluster-level contrastive loss and intra-views cluster-level contrastive loss.

- Inter-views Cluster-level contrastive loss, denoted as $\mathcal{L}_C^{(inter)}$, which is defined as:

$$\mathcal{L}_C^{(inter)} := -\frac{z_i \tilde{u}_{\omega(I_i)}}{\|z_i\|_2 \|\tilde{u}_{\omega(I_i)}\|_2}, \quad (3)$$

where $\omega(I_i)$ is to find the cluster index ℓ for z_i , and \tilde{u}_ℓ is the center vector of the ℓ -th cluster in which $\tilde{\mathcal{U}} := \{\tilde{u}_1, \dots, \tilde{u}_{m'}\}$ and the cluster center \tilde{u}_ℓ is defined as

$$\tilde{u}_\ell = \frac{1}{|\mathcal{C}^{(\ell)}|} \sum_{I_i \in \mathcal{C}^{(\ell)}} \tilde{v}_i, \quad (4)$$

where \tilde{v}_i is the instance feature of image \tilde{I}_i in the instance memory bank $\tilde{\mathcal{M}}$. The inter-views cluster-level contrastive loss $\mathcal{L}_C^{(inter)}(x_i)$ defined in Eq. (3) is used to reduce the discrepancy between the projection output z_i of the first network branch and the cluster center \tilde{u}_ℓ of the feature output of the second branch with the gray-scale view, where $\ell = \omega(I_i)$.

- Intra-views Cluster-level contrastive loss, denoted as $\mathcal{L}_C^{(intra)}$, which is defined as:

$$\mathcal{L}_C^{(intra)} = -(1 - q_i)^2 \ln(q_i) - (1 - \tilde{q}_i)^2 \ln(\tilde{q}_i), \quad (5)$$

where q_i and \tilde{q}_i are the softmax of the inner product of the network outputs and the corresponding instance memory bank, which are defined as

$$q_i = \frac{\exp(\mathbf{u}_{\omega(I_i)}^\top \mathbf{x}_i / \tau)}{\sum_{\ell=1}^{m'} \exp(\mathbf{u}_\ell^\top \mathbf{x}_i / \tau)}, \quad (6)$$

$$\tilde{q}_i = \frac{\exp(\tilde{\mathbf{u}}_{\omega(I_i)}^\top \tilde{\mathbf{x}}_i / \tau)}{\sum_{\ell=1}^{m'} \exp(\tilde{\mathbf{u}}_\ell^\top \tilde{\mathbf{x}}_i / \tau)}, \quad (7)$$

where \mathbf{u}_ℓ and $\tilde{\mathbf{u}}_\ell$ are the center vectors of the ℓ -th cluster for the first branch and the second branch, respectively, in which $\tilde{\mathbf{u}}_\ell$ is defined in (4) and \mathbf{u}_ℓ is defined as

$$\mathbf{u}_\ell = \frac{1}{|\mathcal{C}^{(\ell)}|} \sum_{I_i \in \mathcal{C}^{(\ell)}} \mathbf{v}_i. \quad (8)$$

where \mathbf{v}_i is the instance feature of image \hat{I}_i in the instance memory bank \mathcal{M} . Note that both \mathbf{x}_i and $\tilde{\mathbf{x}}_i$ share the same pseudo labels $\ell = \omega(I_i)$ from clustering. The intra-views cluster-level contrastive loss $\mathcal{L}_C^{(intra)}$ in Eq. (5) is used to encourage the siamese network to learn features with respect to the corresponding cluster center for the two branches, respectively.

Putting the two components together, we have the cluster-level contrastive loss \mathcal{L}_C as follows:

$$\mathcal{L}_C = \mathcal{L}_C^{(inter)} + \mathcal{L}_C^{(intra)}. \quad (9)$$

Remark. Note that the cluster-level contrastive loss \mathcal{L}_C in (9) aims to leverage the cluster structure to minimize the difference between samples of the same category between different augmented views, i.e., via $\mathcal{L}_C^{(inter)}$ in (3), and within the same augmented view, i.e., via $\mathcal{L}_C^{(intra)}$ in (5). This will help the siamese network to further mine the hidden information brought by the basic augmented view in the first branch and the gray-scale augmented view in the second branch.

3.3. Training Procedure for Our CACL Approach

In CACL, the two branches in the siamese network is implemented with ResNet-50 [17]. We pre-train the two network branches respectively on ImageNet at first, and use the learned features to initialize the two memory banks \mathcal{M} and $\tilde{\mathcal{M}}$.

Algorithm 1 Training Procedure for CACL

Input: Given a dataset $\mathcal{I} = \{I_i\}_{i=1}^N$.

Output:

- 1: Initialize the two instance memory banks \mathcal{M} and $\tilde{\mathcal{M}}$ with the output of the two network branches pre-trained on ImageNet, and the model performance $P_{best} = 0$.
 - 2: **while** epoch \leq total epoch **do**
 - 3: Generate \hat{I}_i and \tilde{I}_i via data augmentation $\mathcal{T}(\cdot)$ and $\mathcal{G}(\mathcal{T}'(\cdot))$;
 - 4: Feature extraction to get \mathbf{x}_i and $\tilde{\mathbf{x}}_i$;
 - 5: Clustering and clustering refinement via Eq. (1) to yield pseudo label $\mathcal{Y} = \{\mathbf{y}_1, \dots, \mathbf{y}_N\}$;
 - 6: Update the two cluster centers \mathcal{U} and $\tilde{\mathcal{U}}$ via Eq. (8);
 - 7: Training siamese network to update Θ , Ψ and Θ' via the total loss in Eq. (10);
 - 8: Update instance memory bank \mathcal{M} and $\tilde{\mathcal{M}}$ via Eq. (11) and Eq. (12);
 - 9: Evaluate the model performance P with $F(\cdot|\Theta)$;
 - 10: **if** $P > P_{best}$ **then**
 - 11: Output the best model $F(\cdot|\Theta)$
 - 12: $P_{best} \leftarrow P$
 - 13: **end if**
 - 14: **end while**
-

In the training stage, we train both network branches at the same time with the total loss as follows:

$$\mathcal{L} = \mathcal{L}_I + \mathcal{L}_C = \mathcal{L}_I + \mathcal{L}_C^{(inter)} + \mathcal{L}_C^{(intra)}. \quad (10)$$

We update the two instance memory banks \mathcal{M} and $\tilde{\mathcal{M}}$ as follows:

$$\mathbf{v}_i^{(t)} \leftarrow \alpha \mathbf{v}_i^{(t-1)} + (1 - \alpha) \mathbf{x}_i, \quad (11)$$

$$\tilde{\mathbf{v}}_i^{(t)} \leftarrow \alpha \tilde{\mathbf{v}}_i^{(t-1)} + (1 - \alpha) \tilde{\mathbf{x}}_i, \quad (12)$$

where we set $\alpha = 0.2$ by default.

To prevent collapse², we also use a stop-gradient operation as mentioned in SimSiam [5].

Note that we adopt the stopGrad operation [5] to the second network branch $F'(\cdot|\Theta')$ when using the instance level loss \mathcal{L}_I in (2) to perform back propagation. Thus, the parameters Θ' in the second network branch are updated only with the intra-views cluster-level contrastive loss $\mathcal{L}_C^{(intra)}$ in (5).

For clarity, we summarize the details of the procedure to train our CACL approach in Algorithm 1.

²Note that it is not necessary to use the stop-gradient operation in our CACL because the clustering structure provides enough guide information under the asymmetric structure. Nevertheless, when we train with the symmetric structure as shown in Supporting Materials, the stop-gradient operation is necessary to prevent the collapse.

4. Experiments

To validate the effectiveness of our proposal, we conduct extensive experiments on three benchmark datasets.

4.1. Dataset Description

To evaluate the effectiveness of our proposal, we use the following three benchmark datasets: Market-1501 [39], DukeMTMC-ReID [27] and MSMT17 [32].

Market-1501 has 32668 photos of 1501 people from six different camera views. In the training set, there are of 751 identities with 12936 images. In the testing set, and 19732 images of 750 identities are used for testing. The dataset DukeMTMC-ReID is a large image dataset and it is extracted from the DukeMTMC-ReID video dataset.

DukeMTMC-ReID consists of images sampling from DukeMTMC-ReID video dataset, 120 frames per video, with a total of 36,411 images of people from 1404 different identities. There are 16522 images from 702 identities in the training set and the testing set contains 2228 query images of 702 identities and 17,661 gallery images. These images are composed of eight cameras taken together.

MSMT17 has a total of 126441 images under 15 camera views. In the training set, there are 1041 identities with 32621 images. In the testing set, and 93820 images of 3060 identities are used for testing. The MSMT17 is greatly challenger and larger than the Market-1501 and DukeMTMC datasets.

4.2. Implementation Details

Settings for Training . In our siamese network, we use ResNet-50 [17] pre-trained on the ImageNet [20] for both branches. The feature outputs $\mathbf{x}_i \in \mathbb{R}^D$ and $\tilde{\mathbf{x}}_i \in \mathbb{R}^D$ of the two networks $F(\cdot|\Theta)$ and $F(\cdot|\Theta')$ are D -dimensional vectors where $D = 2048$. We use the features output \mathbf{x}_i of the first branch $F(\cdot|\Theta)$ to perform clustering, where $\mathbf{x}_i = F(\hat{I}_i|\Theta) \in \mathbb{R}^D$. The prediction layer $G(\cdot)$ is a $D \times D$ full connection layer. We initialize the two memory banks with the features outputs from the corresponding network branches $F(\cdot|\Theta)$ and $F'(\cdot|\Theta')$, respectively. We optimize the network through Adam optimizer [19] with a weight decay of 0.0005 and train the network with in total 80 epochs. We change the learning rate dynamically where the learning rate is initially set as 0.00035 and decreased to one-tenth of the previous every 20 epochs. The batch size is set to 64. The temperature coefficient τ in Eq. (7) is set to 0.05 and the update factor α in Eq. (11) and Eq. (12) is set to 0.2.

Setting for Data Augmentation . In our experiments, we use the same data augmentation methods as in SpCL [14], including random horizontal flip, random erasing and random crop.

Setting for Clustering . We use DBSCAN [8] algorithm to generate the raw clusters \mathcal{C} and to generate the over-

Method	Type	Reference	Market-1501				DukeMTMC-ReID			
			mAP	rank-1	rank-5	rank-10	mAP	rank-1	rank-5	rank-10
PTGAN [31]	UDA	CVPR'18	15.7	38.6	57.3	-	13.5	27.4	43.6	-
SPGAN [6]	UDA	CVPR'18	26.7	58.1	76.0	82.7	26.4	46.9	62.6	68.5
TJ-AIDL [30]	UDA	CVPR'18	26.5	58.2	74.8	-	23.0	44.3	59.6	-
PGPPM [34]	UDA	CVPR'18	33.9	63.9	81.1	86.4	17.9	36.3	54.0	61.6
HHL [41]	UDA	ECCV'18	31.4	62.2	78.0	84.0	27.2	46.9	61.0	66.7
SSG [11]	UDA	ECCV'19	58.3	80.0	90.0	92.4	53.4	73.0	80.6	83.2
AD-cluster [37]	UDA	CVPR'20	68.3	86.7	94.4	96.5	54.1	72.6	82.5	85.5
ADTC [18]	UDA	ECCV'20	59.7	79.3	90.8	94.1	52.5	71.9	84.1	87.5
MMCL [29]	UDA	CVPR'20	60.4	84.4	92.8	95.0	51.4	72.4	82.9	85.0
MMT [13]	UDA	ICLR'20	73.8	89.5	96.0	97.6	62.3	76.3	87.7	91.2
JVTC [38]	UDA	ECCV'20	67.2	86.8	95.2	97.1	66.5	80.4	89.9	93.7
MEB [38]	UDA	ECCV'20	76.0	89.9	95.2	96.9	65.3	81.2	90.9	92.2
NRMT [38]	UDA	ECCV'20	71.7	87.8	94.6	96.5	62.2	77.8	86.9	89.5
SpCL [14]	UDA	NIPS'20	76.7	90.3	96.2	97.7	68.8	82.9	90.1	92.5
CAMEL [35]	US	ICCV'17	26.3	54.4	73.1	79.6	19.8	40.2	57.5	64.9
Bow [39]	US	ICCV'15	14.8	35.8	52.4	60.3	8.5	17.1	28.8	34.9
PUL [9]	US	TOMM'18	22.8	51.5	70.1	76.8	22.3	41.1	46.6	63.0
LOMO [22]	US	CVPR'15	8.0	27.2	41.6	49.1	4.8	12.3	21.3	26.6
BUC [23]	US	AAAI'19	30.6	61.0	71.6	76.4	21.9	40.2	52.7	57.4
HCT [36]	US	CVPR'20	56.4	80.0	91.6	95.2	50.1	69.6	83.4	87.4
SSL [24]	US	CVPR'20	37.8	71.7	83.8	87.4	28.6	52.5	63.5	68.9
SpCL [14]	US	NIPS'20	73.1	88.1	96.3	97.7	65.3	81.2	90.3	92.2
CACL	US	This paper	80.9	92.7	97.4	98.5	69.6	<u>82.6</u>	91.2	93.8

Table 1. Comparison to other state-of-the-art. 'UDA' is to refer the unsupervised domain adaptation methods and 'US' is to refer the purely unsupervised learning methods.

segmentation. The DBSCAN algorithm is based on the density of samples. It regards a data point as *density reachable* if the data point lies within a small distance (denoted as d) to other neighboring samples. The parameter d for the maximum distance between neighbor points is the most important parameter in DBSCAN. In experiments, for fair comparison, we follow [14] to set $d = 0.6$ to yield the raw clustering result \mathcal{C} and use a slightly smaller parameter $d = 0.58$ to yield smaller clusters as over-segmentation for cluster refinement.

Metrics for Evaluation. In evaluation, we use the mean average precision (mAP) and cumulative matching characteristic (CMC) at rank-1, 5, 10.

4.3. Comparison to the State-of-the-art

We compare our proposed CACL to the state-of-the-art unsupervised domain adaptation methods and purely unsupervised methods for person Re-ID. The purely unsupervised methods for person Re-ID include: CAMEL [35], PUL [9], SSL [24], LOMO [22], BOW [39], BUC [23], HCT [36], and SpCL [14]. The unsupervised domain adaptation methods for person Re-ID include: PTGAN [31], ADTC [18], HHL [41], SSG [11], MMCL [29], AD-Cluster [37], MEB [38], NRMT [10], SPGAN [6], TJ-AIDL [30], JVTC [21], PGPPM [34], and MMT [13].

The comparison results of the state-of-the-art unsupervised domain adaptation methods and purely unsupervised methods are shown in Table 1. We can find that our proposed CACL achieve 80.9/92.7% at mAP/rank-1 on Market-1501 and 69.6/82.6% at mAP/rank-1 on DukeMTMC. It can be found that we not only perform better than all pure unsupervised methods and also achieve best performance than unsupervised domain adaptation methods. Moreover, we also conduct experiments on a much larger dataset MSMT17 and report the experimental results in Table 2. Again, we can observe that our proposed CACL approach achieve a leading performance, i.e., 21.0/45.4% at mAP/rank-1. It is worth to note that our CACL yields superior performance than the UDA methods on this challenging dataset. These results clearly confirm the effectiveness of our proposal.

4.4. Ablation Study

To evaluate the effectiveness of each component: \mathcal{L}_I , $\mathcal{L}_C^{(inter)}$, $\mathcal{L}_C^{(intra)}$ and clustering with refinement in our CACL approach, we conduct a set of ablation experiments on dataset Market-1501³.

To evaluate the contribution of each component, we conduct a set of experiments by disabling each component in

³We provide more ablation study results in the Support Material.

Method	Type	Reference	MSMT17			
			mAP	rank-1	rank-5	rank-10
PTGAN [31]	UDA	CVPR'18	3.3	11.8	-	27.4
ECN [42]	UDA	CVPR'19	10.2	30.2	41.5	46.8
SSG [11]	UDA	ICCV'19	13.3	32.2	-	51.2
MMCL [29]	UDA	CVPR'20	16.2	43.6	54.3	58.9
JVTC+ [21]	US	ECCV'20	17.3	43.1	53.8	59.4
SpCL [14]	US	NIPS'20	19.1	42.3	55.6	61.2
CACL	US	This paper	21.0	45.4	58.2	63.6

Table 2. Experimental Results on MSMT17.

our CACL framework individually, i.e., CACL w/o cluster refinement, w/o instance-level contrastive loss \mathcal{L}_I and w/o cluster-level contrastive loss \mathcal{L}_C . To further evaluate the sub-part of the cluster-level contrastive loss, we also conduct experiments to evaluate the influence of disabling $\mathcal{L}_C^{(inter)}$ and $\mathcal{L}_C^{(intra)}$, respectively.

We note that the second branch $F'(\cdot|\Theta')$ is trained only with $\mathcal{L}_C^{(intra)}$. Thus, in the ablation experiments, when disabling the cluster-level contrastive loss \mathcal{L}_C and the sub-part of $\mathcal{L}_C^{(intra)}$, we need to modify the loss in Eq. (5) to keep the part only involving the second network branch as follows:

$$\tilde{\mathcal{L}}_C^{(intra)} := -(1 - \tilde{q}_i)^2 \ln(\tilde{q}_i). \quad (13)$$

When disabling both \mathcal{L}_C and \mathcal{L}_I , we just use the Eq. (13) to train the single branch with data augmentation $\mathcal{T}'(\cdot)$. The results of the ablation study are reported in Table 3.

As can be read in Table 3, the performance drops when one component is disabled individually. This validates that each component contributes to the performance improvements. In the experiments without using $\mathcal{L}_C^{(intra)}$, the performance of our CACL drops the most significantly. This is because that, as we mentioned above, $\mathcal{L}_C^{(intra)}$ is used to keep the features of the same cluster be close for each data augmentation view, and $\mathcal{L}_C^{(inter)}$ is used to learn the feature distribution between different data augmentation views. If the first branch trains with $\mathcal{L}_C^{(inter)}$ without using $\mathcal{L}_C^{(intra)}$, it will pay more attention on the features from gray-scale views and ignore the features from color views, thus the performance degenerates. More interpretation and evaluation are provided in Supporting Materials.

4.5. More Evaluation and Analysis

To validate the effectiveness of using a gray-scale process $\mathcal{G}(\cdot)$ over the data augmentation $\mathcal{T}'(\cdot)$ for the second network branch, we conduct a set of experiments under different settings: a) simply using data augmentation $\mathcal{T}'(\cdot)$ without using gray-scale transform $\mathcal{G}(\cdot)$; b) using another data augmentation approach, named color-jitter, which denoted as $\mathcal{J}(\cdot)$ to replace $\mathcal{G}(\cdot)$, which output is still a color image; c) with gray-scale transform $\mathcal{G}(\cdot)$ after $\mathcal{T}'(\cdot)$. We display the image samples processed with different data

Components	Market-1501			
	mAP	rank-1	rank-5	rank-10
Ours w/o \mathcal{L}_I & \mathcal{L}_C	68.1	85.2	94.0	96.0
Ours w/o cluster refine	73.4	88.5	94.7	96.8
Ours w/o \mathcal{L}_I	80.4	92.2	97.1	98.2
Ours w/o \mathcal{L}_C	76.6	90.1	96.3	97.4
Ours w/o $\mathcal{L}_C^{(intra)}$	45.6	68.2	83.8	88.3
Ours w/o $\mathcal{L}_C^{(inter)}$	80.4	92.2	96.5	97.8
Our CACL	80.9	92.7	97.4	98.5

Table 3. Ablation Study on Market-1501.

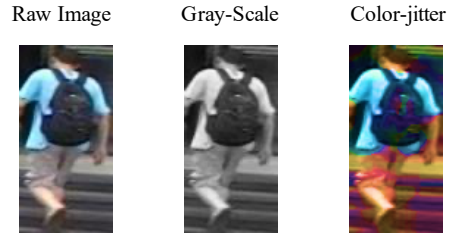


Figure 4. Effects of Using Color-jitter vs. Gray-scale

Components	Market-1501			
	mAP	rank-1	rank-5	rank-10
Data augmentation $\mathcal{T}'(\cdot)$	79.0	90.6	96.3	97.1
Color-jitter $\mathcal{J}(\mathcal{T}'(\cdot))$	79.1	90.8	96.7	97.8
Gray-scale $\mathcal{G}(\mathcal{T}'(\cdot))$	80.9	92.7	97.4	98.5

Table 4. Performance Comparison on using Color Data Augmentations and Gray-scale Transform to the Second Network Branch.

augmentation methods in Fig. 4. As can be observed, color-jitter did change the image, but the color information still dominates.

Experimental results are provided in Table 4. We can find that using color-jitter did not significantly improve the performance compared to using data augmentation $\mathcal{T}'(\cdot)$ itself. This is because that color-jitter does not really eliminate the influence of color, that is, the original similar color is still similar after changing the hue. This also validates that our ideas and methods are correct and effective to improve the model performance.

To further reveal the performance of the trained networks, we record the performance of using the features of each branch of two networks $F(\cdot|\Theta)$ and $F'(\cdot|\Theta')$ for person Re-ID in Table 5. We can read that using the second branch $F'(\cdot|\Theta')$ did yield significantly lower performance than that of using the first branch $F(\cdot|\Theta)$, and the result of $F'(\cdot|\Theta')$ is similar to the result of experiments without using $\mathcal{L}_C^{(intra)}$. This is because that the second network branch pays attention on learning features from gray-scale images, lacking of the ability to capture richer information from color images.

Branch	Market-1501			
	mAP	rank-1	rank-5	rank-10
$F(\cdot \Theta)$ (Color)	80.9	92.7	97.4	98.5
$F'(\cdot \Theta')$ (Gray-Scale)	43.8	71.5	83.9	87.1

Table 5. Performance Comparison on $F(\cdot|\Theta)$ and $F'(\cdot|\Theta')$.

5. Conclusion

We have proposed a Cluster-guided Asymmetric Contrastive Learning (CACL) approach for unsupervised person Re-ID, in which cluster structure is leveraged to guide the feature learning in a properly designed contrastive learning framework. Specifically, in our proposed CACL, instance-level contrastive learning is conducted with respect to the asymmetric data augmentation and cluster-level contrastive learning is conducted with respect to the clustering structure. By leveraging the cluster structure into contrastive learning, CACL is able to effectively exploit the invariance within and between different data augmentation views for learning more effective feature beyond the dominating colors. We have conducted extensive experiments on three benchmark datasets and demonstrated the superior performance of our proposal.

References

- [1] Slawomir Bak, Peter Carr, and Jean-Francois Lalonde. Domain adaptation through synthesis for unsupervised person re-identification. In *European Conference on Computer Vision*, pages 189–205, 2018. 3
- [2] Piotr Bojanowski and Armand Joulin. Unsupervised learning by predicting noise. In *International Conference on Machine Learning*, pages 517–526. PMLR, 2017. 3
- [3] Mathilde Caron, Ishan Misra, Julien Mairal, Priya Goyal, Piotr Bojanowski, and Armand Joulin. Unsupervised learning of visual features by contrasting cluster assignments. *arXiv preprint arXiv:2006.09882*, 2020. 2, 3
- [4] Ting Chen, Simon Kornblith, Mohammad Norouzi, and Geoffrey Hinton. A simple framework for contrastive learning of visual representations. In *International conference on machine learning*, pages 1597–1607, 2020. 2, 3, 5
- [5] Xinlei Chen and Kaiming He. Exploring simple siamese representation learning. *arXiv preprint arXiv:2011.10566*, 2020. 2, 3, 6, 11
- [6] Weijian Deng, Liang Zheng, Qixiang Ye, Guoliang Kang, Yi Yang, and Jianbin Jiao. Image-image domain adaptation with preserved self-similarity and domain-dissimilarity for person re-identification. In *IEEE Conference on Computer Vision and Pattern Recognition*, pages 994–1003, 2018. 7
- [7] Alexey Dosovitskiy, Philipp Fischer, Jost Tobias Springenberg, Martin Riedmiller, and Thomas Brox. Discriminative unsupervised feature learning with exemplar convolutional neural networks. *IEEE transactions on pattern analysis and machine intelligence*, 38(9):1734–1747, 2015. 3
- [8] Martin Ester, Hans-Peter Kriegel, Jörg Sander, and Xiaowei Xu. A density-based algorithm for discovering clusters in large spatial databases with noise. In *Proceedings of the Second International Conference on Knowledge Discovery and Data Mining*, page 226–231, 1996. 2, 4, 6
- [9] Hehe Fan, Liang Zheng, Chenggang Yan, and Yi Yang. Unsupervised person re-identification: Clustering and fine-tuning. *ACM Transactions on Multimedia Computing, Communications, and Applications*, 14(4):83, 2018. 3, 7
- [10] Zhao Fang, Liao Shengcai, Xie Guosen, Zhao Jian, Zhang Kaihao, and Ling Shao. Unsupervised domain adaptation with noise resistible mutual-learning for person re-identification. In *European Conference on Computer Vision*, 2020. 7
- [11] Yang Fu, Yunchao Wei, Guanshuo Wang, Yuqian Zhou, Honghui Shi, and Thomas S. Huang. Self-similarity grouping: A simple unsupervised cross domain adaptation approach for person re-identification. In *The IEEE International Conference on Computer Vision*, October 2019. 2, 7, 8
- [12] Yaroslav Ganin and Victor Lempitsky. Unsupervised domain adaptation by backpropagation. *arXiv preprint arXiv:1409.7495*, 2014. 3
- [13] Yixiao Ge, Dapeng Chen, and Hongsheng Li. Mutual mean-teaching: Pseudo label refinery for unsupervised domain adaptation on person re-identification. In *International Conference on Learning Representations*, 2020. 2, 7
- [14] Yixiao Ge, Feng Zhu, Dapeng Chen, Rui Zhao, and Hongsheng Li. Self-paced contrastive learning with hybrid memory for domain adaptive object re-id. In *Advances in Neural Information Processing Systems*, 2020. 3, 4, 6, 7, 8
- [15] Jean-Bastien Grill, Florian Strub, Florent Altché, Corentin Tallec, Pierre Richemond, Elena Buchatskaya, Carl Doersch, Bernardo Avila Pires, Zhaohan Guo, Mohammad Gheshlaghi Azar, Bilal Piot, koray kavukcuoglu, Remi Munos, and Michal Valko. Bootstrap your own latent - a new approach to self-supervised learning. In H. Larochelle, M. Ranzato, R. Hadsell, M. F. Balcan, and H. Lin, editors, *Advances in Neural Information Processing Systems*, volume 33, pages 21271–21284. Curran Associates, Inc., 2020. 2, 3, 5
- [16] Kaiming He, Haoqi Fan, Yuxin Wu, Saining Xie, and Ross Girshick. Momentum contrast for unsupervised visual representation learning. In *Conference on Computer Vision and Pattern Recognition*, June 2020. 3
- [17] Kaiming He, Xiangyu Zhang, Shaoqing Ren, and Jian Sun. Deep residual learning for image recognition. In *IEEE Conference on Computer Vision and Pattern Recognition*, pages 770–778, 2016. 4, 5, 6
- [18] Zilong Ji, Xiaohan Zou, Xiaolongand Lin, Xiao Liu, Tiejun Huang, and Si Wu. An attention-driven two-stage clustering method for unsupervised person re-identification. In *European Conference on Computer Vision*, 2020. 7
- [19] Diederik P Kingma and Jimmy Ba. Adam: A method for stochastic optimization. *arXiv preprint arXiv:1412.6980*, 2014. 6
- [20] Alex Krizhevsky, Ilya Sutskever, and Geoffrey E Hinton. Imagenet classification with deep convolutional neural networks. In *Conference and Workshop on Neural Information Processing Systems*, pages 1097–1105, 2012. 4, 6

- [21] Jianing Li and Shiliang Zhang. Joint visual and temporal consistency for unsupervised domain adaptive person re-identification. In *European Conference on Computer Vision*, 2020. 7, 8
- [22] Shengcai Liao, Yang Hu, Xiangyu Zhu, and Stan Z Li. Person re-identification by local maximal occurrence representation and metric learning. In *IEEE Conference on Computer Vision and Pattern Recognition*, pages 2197–2206, 2015. 7
- [23] Yutian Lin, Xuanyi Dong, Liang Zheng, Yan Yan, and Yi Yang. A bottom-up clustering approach to unsupervised person re-identification. In *The Association for the Advancement of Artificial Intelligence*, volume 33, pages 8738–8745, 2019. 3, 7
- [24] Yutian Lin, Lingxi Xie, Yu Wu, Chenggang Yan, and Qi Tian. Unsupervised person re-identification via softened similarity learning. In *IEEE Conference on Computer Vision and Pattern Recognition*, 2020. 3, 7
- [25] Jiawei Liu, Zheng-Jun Zha, Di Chen, Richang Hong, and Meng Wang. Adaptive transfer network for cross-domain person re-identification. In *IEEE Conference on Computer Vision and Pattern Recognition*, pages 7202–7211, 2019. 3
- [26] Peixi Peng, Tao Xiang, Yaowei Wang, Massimiliano Pontil, Shaogang Gong, Tiejun Huang, and Yonghong Tian. Unsupervised cross-dataset transfer learning for person re-identification. In *IEEE Conference on Computer Vision and Pattern Recognition*, pages 1306–1315, 2016. 3
- [27] Ergys Ristani and Carlo Tomasi. Features for multi-target multi-camera tracking and re-identification. In *Proceedings of the IEEE conference on computer vision and pattern recognition*, pages 6036–6046, 2018. 6
- [28] Baochen Sun, Jiashi Feng, and Kate Saenko. Return of frustratingly easy domain adaptation. In *Association for the Advancement of Artificial Intelligence*, 2016. 3
- [29] Dongkai Wang and Shiliang Zhang. Unsupervised person re-identification via multi-label classification. In *Advances in Neural Information Processing Systems*, 2020. 3, 7, 8
- [30] Jingya Wang, Xiatian Zhu, Shaogang Gong, and Wei Li. Transferable joint attribute-identity deep learning for unsupervised person re-identification. In *IEEE Conference on Computer Vision and Pattern Recognition*, pages 2275–2284, 2018. 3, 7
- [31] Longhui Wei, Shiliang Zhang, Wen Gao, and Qi Tian. Person transfer gan to bridge domain gap for person re-identification. In *IEEE Conference on Computer Vision and Pattern Recognition*, pages 79–88, 2018. 7, 8
- [32] Longhui Wei, Shiliang Zhang, Wen Gao, and Qi Tian. Person transfer gan to bridge domain gap for person re-identification. In *Proceedings of the IEEE conference on computer vision and pattern recognition*, pages 79–88, 2018. 6
- [33] Jiahao Xie, Xiaohang Zhan, Ziwei Liu, Yew Soon Ong, and Chen Change Loy. Delving into inter-image invariance for unsupervised visual representations. In *Conference and Workshop on Neural Information Processing Systems*, 2020. 2, 3
- [34] Fengxiang Yang, Zhun Zhong, Zhiming Luo, Sheng Lian, and Shaozi Li. Leveraging Virtual and Real Person for Unsupervised Person Re-identification. *arXiv e-prints*, page arXiv:1811.02074, Nov. 2018. 7
- [35] Hong-Xing Yu, Ancong Wu, and Wei-Shi Zheng. Cross-view asymmetric metric learning for unsupervised person re-identification. In *IEEE International Conference on Computer Vision*, pages 994–1002, 2017. 7
- [36] Kaiwei Zeng, Munan Ning, Yaohua Wang, and Yang Guo. Hierarchical clustering with hard-batch triplet loss for person re-identification. In *IEEE Conference on Computer Vision and Pattern Recognition*, 2020. 2, 3, 7
- [37] Yunpeng Zhai, Shijian Lu, Qixiang Ye, Xuebo Shan, Jie Chen, Rongrong Ji, and Yonghong Tian. Ad-cluster: Augmented discriminative clustering for domain adaptive person re-identification. In *IEEE Conference on Computer Vision and Pattern Recognition*, 2020. 7
- [38] Yunpeng Zhai, Qixiang Ye, Shijian Lu, Mengxi Jia, Rongrong Ji, and Yonghong Tian. Multiple expert brainstorming for domain adaptive person re-identification. In *European Conference on Computer Vision*, 2020. 7
- [39] Liang Zheng, Liyue Shen, Lu Tian, Shengjin Wang, Jingdong Wang, and Qi Tian. Scalable person re-identification: A benchmark. In *IEEE International Conference on Computer Vision*, pages 1116–1124, 2015. 6, 7
- [40] Liang Zheng, Yi Yang, and Alexander G Hauptmann. Person re-identification: Past, present and future. *arXiv preprint arXiv:1610.02984*, 2016. 1, 3
- [41] Zhun Zhong, Liang Zheng, Shaozi Li, and Yi Yang. Generalizing a person retrieval model hetero-and homogeneously. In *European Conference on Computer Vision*, pages 172–188, 2018. 7
- [42] Zhun Zhong, Liang Zheng, Zhiming Luo, Shaozi Li, and Yi Yang. Invariance matters: Exemplar memory for domain adaptive person re-identification. In *IEEE Conference on Computer Vision and Pattern Recognition*, 2019. 8

Appendices

In this supplementary materials, we provide more experimental results, including evaluation on a variant of our CACL framework, i.e., Cluster-guided Symmetric Contrastive Learning (CSCL), more complete ablation studies, and a data visualization experiment.

A. Variant of Our CACL: Cluster-guided Symmetric Contrastive Learning (CSCL)

We note that our proposed CACL uses an asymmetric structure to perform contrastive learning. Here, we modify the framework of CACL by adding two extra contrastive learning modules: instance-level contrastive learning via \mathcal{L}'_I and cluster-level contrastive learning via \mathcal{L}'_C , as shown in Fig. 3. Due to the symmetric structure in contrastive learning, we refer the modified framework a Cluster-guided Symmetric Contrastive Learning (CSCL).

To be specific, as shown in Fig. 3, we add another predictor layer $G'(\cdot|\Psi')$ after the second network branch to construct a symmetric structure for contrastive learning and adopt an instance-level contrastive loss \mathcal{L}'_I which is defined as follows:

$$\mathcal{L}'_I = -\frac{\tilde{z}'_i{}^\top \mathbf{x}_i}{\|\tilde{z}'_i\|_2 \|\mathbf{x}_i\|_2}. \quad (14)$$

We also modify the inter-views cluster-level contrastive loss $\mathcal{L}_C^{(inter)}$ by adding a new component $\mathcal{L}'_C^{(inter)}$, which is defined as:

$$\mathcal{L}'_C^{(inter)} = -\frac{\tilde{z}'_i{}^\top \mathbf{u}_i}{\|\tilde{z}'_i\|_2 \|\mathbf{u}_i\|_2}. \quad (15)$$

It should be noted that when using the stop-gradient strategy [5], we only updates the parameters in the second network branch with \mathcal{L}'_C .

A.1. Performance Comparison between Symmetric Structure vs. Asymmetric Structure

We conduct experiments on Market-1501 to evaluate the performance of the symmetric structure in CSCL and the asymmetric structure in CACL. To make a fair comparison, we keep all the settings the same. The experimental results are reported in Table 6. We can read that the additional parts in the symmetric network structure does bring slightly improvement but the improvement is not significant. Nevertheless, the additional parts to form the symmetric structure did make the network more complicated because a new predictor layer is added. Thus, we prefer to use the asymmetric structure, in order to keep the framework as simple as possible.

A.2. More Ablation Study

In this subsection, we provide more complete ablation study results in Table 7. We add a set of experiments, including CACL without (w/o) clustering, CACL w/o stop-gradient, and CSCL (symmetric structure) w/o stop-gradient. It should be noted that when CACL is trained without using clustering module, it is trained with \mathcal{L}_I . As can be read from the first row in the results, the performance is as worse as random guess. We think that simply using the instance-level contrastive loss \mathcal{L}_I to perform contrastive learning is hardly to help the network to learn distinguishable features. This justifies the necessity of guiding the contrastive learning with clusters.

Moreover, we also test the stop-gradient operations under different structures. As can be read that, the performance of the framework with symmetric structure drops significantly when the stop-gradient operation is not used; whereas the performance of the framework with asymmetric structure drops slightly (i.e., only 0.7% lower than using the stop-gradient operation) when the stop-gradient operation is not used. Thus, the stop-gradient operation is necessary to maintain the difference of two branches to train the framework with symmetric structure; whereas the framework with asymmetric structure in CACL does not highly depend on the stop-gradient operation.

Components	Market-1501			
	mAP	rank-1	rank-5	rank-10
CACL	80.9	92.7	97.4	98.5
CSCL	81.0	93.0	97.2	98.3

Table 6. Performance Comparison between Asymmetric Structure (CACL) and Symmetric Structure (CSCL)

A.3. Data Visualization

To gain some intuitive understanding of the performance of our proposed CACL, we conduct a data visualization experiment on Market-1501 to visualize the clustering results

Components	Market-1501			
	mAP	rank-1	rank-5	rank-10
CACL w/o clustering	0.3	0.5	1.2	2.3
CACL w/o \mathcal{L}_I & \mathcal{L}_C	68.1	85.2	94.0	96.0
CACL w/o cluster refine	73.4	88.5	94.7	96.8
CACL w/o \mathcal{L}_I	80.4	92.2	97.1	98.2
CACL w/o \mathcal{L}_C	76.6	90.1	96.3	97.4
CACL w/o \mathcal{L}_C^{intra}	45.6	68.2	83.8	88.3
CACL w/o \mathcal{L}_C^{inter}	80.4	92.2	96.5	97.8
CACL w/o <i>stopGrad</i>	80.2	92.0	97.0	97.6
CSCL w/o <i>stopGrad</i>	15.0	31.7	46.5	54.2
Our CACL	80.9	92.7	97.4	98.5

Table 7. Ablation Study on Market-1501.

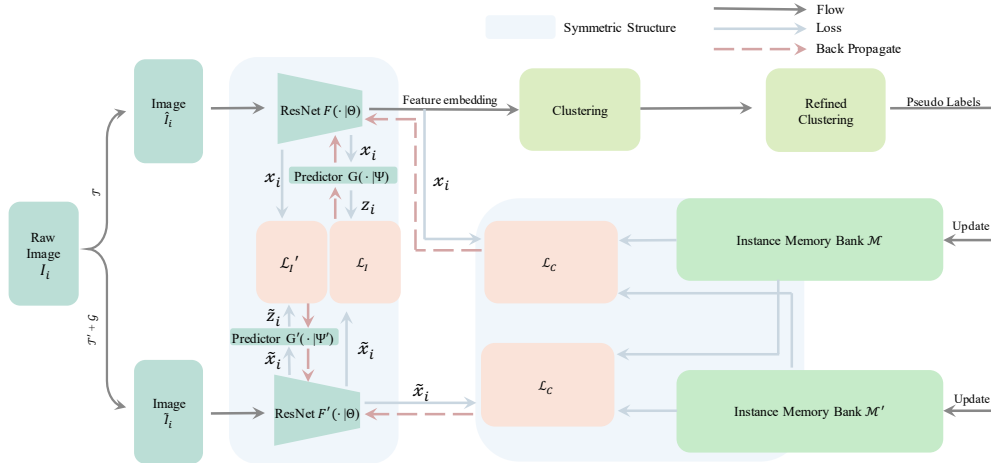


Figure 5. Illustration of Cluster-guided Symmetric Contrastive Learning Framework. The symmetric structures are marked in light blue shadow.

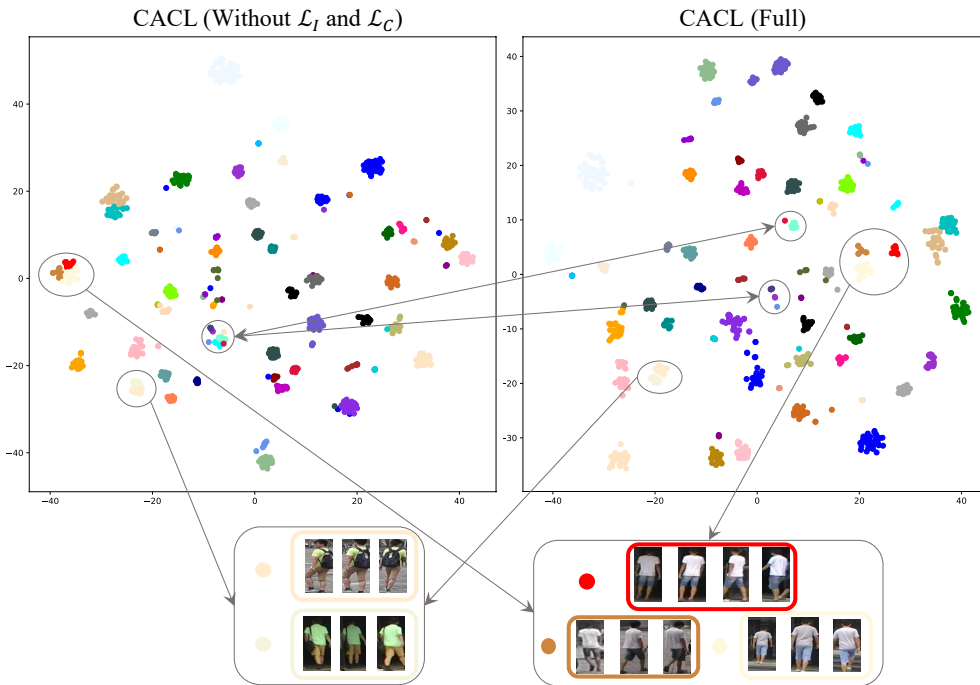


Figure 6. Data Visualization (via t -SNE) of the learned feature and clusters under two different training strategies: Training without \mathcal{L}_C and \mathcal{L}_I (left) as mentioned in Table 3 and our CACL (right). The data points come from the Market-1501 training set (1,000 images of 60 identities). The points with the same color mean the image of the same identity. To demonstrate the difference between the two distributions in details, we further zoom in the circled clusters and show the corresponding images. The images in the boxes are similar to each other and the corresponding data points are very close to each other or even overlapping in the feature space if the model is trained without using \mathcal{L}_C and \mathcal{L}_I , as shown in the left box; whereas the contrastive losses will efficient distinguish these data points and maintain the cluster compactness as shown in the right box.

of the learned features when different training strategies are used: a) without using the contrastive losses \mathcal{L}_C and \mathcal{L}_I ; and b) using the contrastive losses \mathcal{L}_C and \mathcal{L}_I .

Experimental results are shown in Fig. 6. We can ob-

serve that the contrastive losses \mathcal{L}_C and \mathcal{L}_I did help the model distinguish those similar images while maintaining the cluster compactness, and also separate the overlapping individual samples from each other.